MOLECULAR PHYSICS, 10–20 DECEMBER 2003, VOL. 101, NOS. 23–24, 3477–3492

Taylor & Francis
Taylor & Francis Group

Complete characterization of the water dimer vibrational ground state and testing the VRT(ASP-W)III, SAPT-5st, and VRT(MCY-5f) surfaces

FRANK N. KEUTSCH[1], NIR GOLDMAN[2], HEATHER A. HARKER[3], CLAUDE LEFORESTIER[4] and RICHARD J. SAYKALLY[3]*

[1]Department of Chemistry and Chemical Biology, Harvard University, Cambridge, MA 02138, USA
[2]Chemistry and Materials Science Directorate, Lawrence Livermore National Lab, L-268, Livermore, CA 94551, USA
[3]Department of Chemistry, University of California, Berkeley, CA 94720, USA
[4]Laboratoire Structure et Dynamique des Systèmes Moléculaire et Solides (UMR 5636), CC014, Université des Sciences et Techniques du Langue-doc, 34095 Montpellier Cédex 05, France

(*Received 14 October 2003; accepted 14 October 2003*)

We report the observation of extensive a- and c-type rotation-tunnelling (RT) spectra of $(H_2O)_2$ for $K_a = 0$–3, and $(D_2O)_2$ for $K_a = 0$–4. These data allow a detailed characterization of the vibrational ground state to energies comparable to those of the low-lying (70–80 cm^{-1}) intermolecular vibrations. We present a comparison of the experimentally determined molecular constants and tunnelling splittings with those calculated on the VRT(ASP-W)III, SAPT-5st, and VRT(MCY-5f) intermolecular potential energy surfaces. The SAPT-5st potential reproduces the vibrational ground state properties of the water dimer very well. The VRT(MCY-5f) and especially the VRT(ASP-W)III potentials show larger disagreements, in particular for the bifurcation tunnelling splitting.

1. Introduction

The study of weakly bound systems with high-resolution spectroscopic methods allows the determination of accurate intermolecular potential energy surfaces [1-8]. Water clusters are of special interest due to the importance of water as a ubiquitous solvent and its role in many important chemical processes [9]. The determination of an accurate potential surface for water has produced much experimental and theoretical interest in water clusters and their structural and dynamical properties [6–8, 10–27]. The most important step towards a determination of such potentials from water cluster spectra is to obtain an accurate water dimer potential, as the two-body forces account for ~80% of the total interaction energy, and the dominant many-body forces (induction) are contained in the tensorial description of polarization [28, 29].

There are actually two related but distinct goals for water dimer potential determinations. The first is the determination of a 'universal potential' for water, which could be used for liquid and solid water, as well as water clusters. The steps toward this consist of determining a dimer potential incorporating a correct description of the induction interaction and subsequent augmentation of this potential with the subtle three-body exchange and dispersion terms, extracted from studies of larger water clusters. The resulting potential should be 'universally' applicable to isolated water clusters as well as to bulk water, and efforts towards obtaining such a potential [6–8] and simulating bulk properties with these [30, 31] are underway. It is expected that this 'universal potential' will sacrifice some accuracy compared to the spectroscopic data for general applicability and simplicity of functional form to make calculations of larger systems computationally feasible. The second goal is the determination of a highly accurate water dimer potential to be used explicitly for the calculation of water dimer properties, such as equilibrium constants

*Author for correspondence. e-mail: saykally@uclink4.berkeley.edu

Molecular Physics ISSN 0026–8976 print/ISSN 1362–3028 online
http://www.tandf.co.uk/journals
DOI: 10.1080/00268970310001636486

[32]. We note that the water dimer has recently been detected in the atmosphere [33], and it has been proposed that the water dimer and other weakly bound systems (e.g. $N_2{\cdot}H_2O$ [34], $O_2{\cdot}H_2O$ [34, 35] and $HO_2{\cdot}H_2O$ [36]) could facilitate a number of atmospherically important chemical reactions. The unequivocal corroboration of the atmospheric observation of the water dimer depends critically on the calculated properties (e.g. vibrational frequencies and intensities and equilibrium concentrations) of the dimer. Clearly, a highly accurate water dimer potential is central to these calculations [32]. Three dimer potentials of spectroscopic accuracy currently exist [6–8, 37] and we have recently presented a comparison of the $(H_2O)_2$ intermolecular vibrational frequencies ($< 150\,cm^{-1}$) calculated on these potentials with experimental results [27]. However, high-lying rotational states of the vibrational ground state can reach energies comparable to those of the lower intermolecular vibrational levels, and it is also important to properly represent these (especially for the calculation of partition functions). The dependence of the tunnelling splittings on rotational quantum numbers is a stringent test for any potential as they sample the overall topography of the potential energy surface and not predominantly the minima, as do the vibrational states. We recently presented a preliminary study with experimental $(D_2O)_2$ results [38], but here we extend the measurements of $(H_2O)_2$ and to a comparison with the three most important, spectroscopically accurate potentials.

2. Background: tunnelling motions of the water dimer

The water dimer (see figure 1) is a highly non-rigid near-prolate top and the rotational spectrum of the vibrational ground state of the water dimer therefore exhibits a large number of rotation-tunnelling splittings resulting from three main tunnelling motions

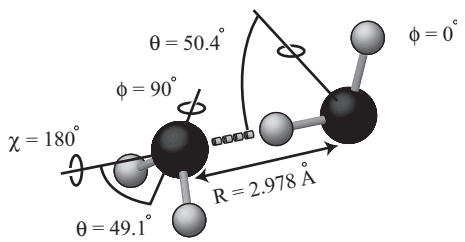

Figure 1. The equilibrium structure of the water dimer determined from the VRT(ASP-W)III surface [37]. The non-rigid structure undergoes a number of large amplitude vibrations and tunnelling motions that exchange the protons of the acceptor water molecule (*a*), interchanges the roles of the acceptor and donor molecules (*i*), or exchange the protons of the donor molecule via a bifurcated transition state (*b* = bifurcation tunnelling).

[12, 14, 19, 24, 25]. These tunnelling splittings are crucial constraints for the fitting and testing of intermolecular water dimer potential energy surfaces as they reflect the overall topography and not just the minima of the potential energy surface. (However, to date no such comparison has been done for the higher K_a levels of the water dimer.) These tunnelling splittings and the group theoretical treatment and selection rules of the water dimer have been described in detail previously and will only be discussed briefly [12, 14, 19, 24, 25]. The tunnelling motion that results in the largest splitting is the acceptor switching splitting, henceforth referred to as '*a*'; the second largest splitting is the interchange splitting, henceforth referred to as '*i*'; and bifurcation tunnelling, henceforth referred to as '*b*', results in a small shift of the dimer energy levels. Figure 2 shows the energy level structure resulting from these tunnelling splittings. The acceptor switching splitting gives rise to one set of energy levels with symmetries $A_1/E_1/B_1$ (henceforth referred to as 1s) and another set of three energy levels with symmetries $A_2/E_2/B_2$ (henceforth referred to as 2s). It should be pointed out that there is no group theoretical relevance to the subscripts of the E symmetries and these act merely as labels.

2.1. *Coriolis interactions*

In the vibrational ground state of $(H_2O)_2$, the 2s of $K_a = 1$ are very close in energy to the 2s of $K_a = 0$. As K_a is not a good quantum number, states with the same overall symmetry are allowed to mix if they have the same J rotational quantum number. A model was proposed which couples the vibrational angular momentum with the overall rotation of the complex [24]. This Coriolis perturbation results in characteristic shifts of all the transitions involving the 2s of $K_a = 0$ of $(H_2O)_2$ and half of the asymmetry doublets of the 2s of $K_a = 1$. Although the spectra are complicated by the Coriolis interaction, the characteristic appearance of the perturbation can aid in the identification and assignment of $(H_2O)_2$ spectra.

Figure 2 shows the correlation diagram of the rotation-tunnelling levels of the water dimer, together with the weights from nuclear spin statistics. The group theoretical treatment and selection rules of the water dimer have been described in detail and the allowed transitions are: $A_1^+ \leftrightarrow A_1^-$, $A_2^+ \leftrightarrow A_2^-$, $B_1^+ \leftrightarrow B_1^-$, $B_2^+ \leftrightarrow B_2^-$ and $E^+ \leftrightarrow E^-$ [11, 12, 14, 16, 19, 25, 39]. It should be emphasized that there is no group theoretical difference between the E_1 and E_2 symmetries shown in figure 2 and the subscripts only act as labels. Transitions between E_1 and E_2 states are allowed, and various authors have calculated the transition dipole moments for these transitions in the vibrational ground state as well as such transitions to excited vibrational states. The

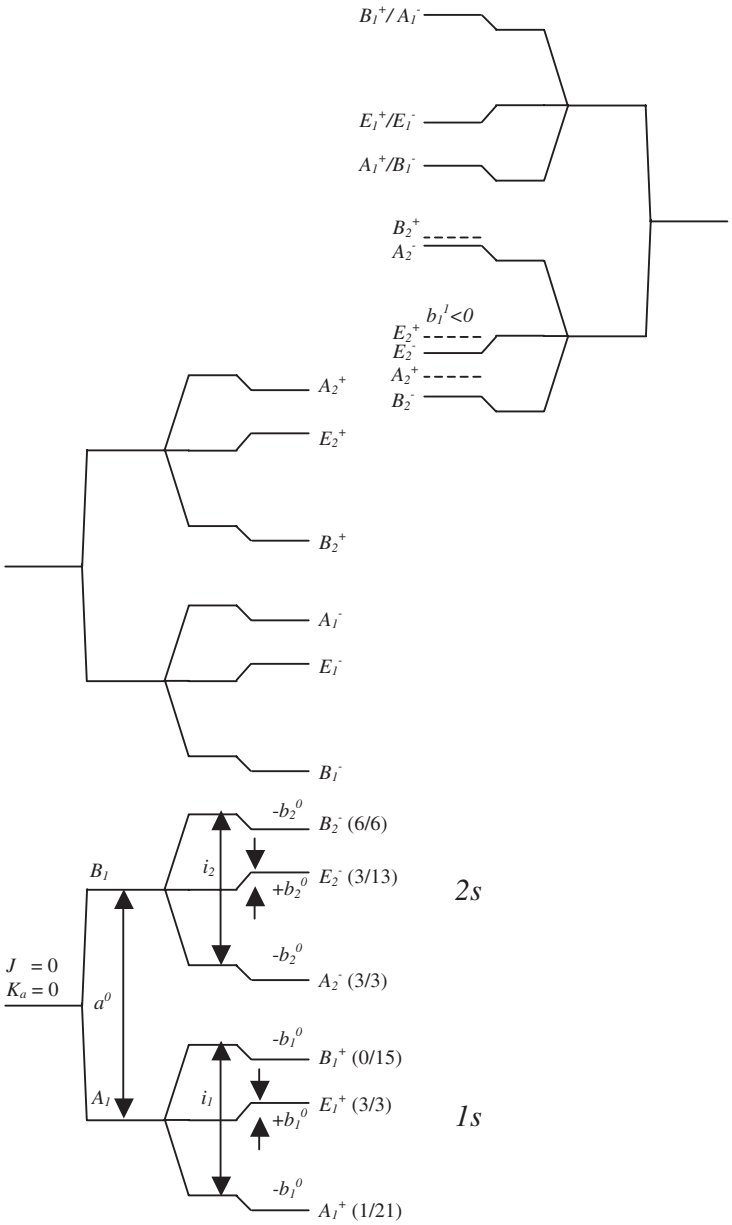

Figure 2. The correlation diagram for the rotation-tunnelling states of $(H_2O)_2$ is shown for $K_a = 0$ and 1 together with the symmetry labels and weights from nuclear spin statistics $[(H_2O)_2/(O_2O)_2]$. The $A_1/E_1/B_1$ levels are referred to as the 1s and the $A_2/E_2/B_2$ as the 2s. The effects of the tunnelling splittings are indicated as well as the Coriolis shifts for $K_a = 1$ (not for $K_a = 0$), but all of these are not drawn to scale. The definition of the tunnelling splittings is as follows:

$$a^K = \frac{1}{4}\left[E^K_{A_2^-/B_2^+} + E^K_{B_2^-/A_2^+} + 2E^K_{E_2}\right] - \frac{1}{4}\left[E^K_{A_1^+/B_1^-} + E^K_{B_1^+/A_1^-} + 2E^K_{E_1}\right],$$

for $J = K_a$;

$$i_1^K = \frac{1}{4}\left[E^K_{B_1^+/A_1^-} - E^K_{A_1^+/B_1^-}\right],$$

for $J = K_a$ of the 1s (analogous expression for the 2s); and

$$b_1^K = \frac{1}{4}\left[2E^K_{E_1} - E^K_{A_1^+/B_1^-} - E^K_{B_1^+/A_1^-}\right],$$

for $J = K_a$ of the 1s (analogous expression for the 2s).

calculations indicate that such transitions should be experimentally observable, but no purely rotational $E_2 \leftrightarrow E_1$-state transitions have been previously observed, although transitions to $K_a = 0$ E_1 states of the donor-torsion vibrational level have been recently proposed [27]. From the selection rules, it follows that tunnelling results in a splitting of each rotational transition into six components, which typically appear as two sets (1s and 2s) of three more closely spaced transitions (e.g. $A_1/E_1/B_1$). The relative intensities are determined by the weights from nuclear spin statistics (shown in figure 2) and rotational transitions can be a-type ($\Delta K_a = 0$) or c-type ($\Delta K_a = \pm 1$) [24, 25].

3. Experiment

The experimental configuration used in the observation of the water dimer data presented here has been described previously [38] and only the principal differences will be discussed here. A millimetre wave synthesizer (KVARZ) with a maximum power of 40 mW was used to generate millimetre radiation between 53 and 118 GHz. The $(D_2O)_2$ transitions at higher frequencies were observed during our investigation of the 583.2 GHz $(D_2O)_3$ band using a BWO configuration described elsewhere [40]. The radiation was detected by a fixed magnetic field InSb bolometer (IR-Labs) after a single pass through a pulsed planar supersonic expansion. Water clusters were formed by expanding pure Ar, or N_2, saturated with H_2O or D_2O, through a 101.6 mm long slit at a repetition rate of 40–50 Hz [41]. The vacuum chamber was maintained at *ca.* 60 mTorr with a Roots blower (Edwards EH4200) backed by two rotary pumps (Edwards E2M275). The initial study investigating transitions originating in $K_a = 0$ and 1 states used Ar as the carrier gas, and exhibited signal-to-noise ratios of *ca.* 10 000 for the a-type $K_a = 0$ transitions of the E_1 states. During the search for transitions of larger K_a, N_2 was used as the carrier gas resulting in a signal-to-noise ratio of 35:1 for the most intense $(D_2O)_2$ $K_a = 3$ transition (R(9) of the $E^{\pm}_{1/2}$ states) originating *ca.* 50 cm^{-1} above the ground state. Figure 3 shows representative spectra for $(H_2O)_2$.

4. Results and comparison with theory

A total of 49 a-type ($\Delta K_a = 0$) transitions of the 1s and 70 a-type and 6 c-type ($\Delta K_a = 1$) transitions of the 2s were observed and assigned for $(H_2O)_2$ and are presented in tables 1–4 together with previously observed transitions. Figure 3 shows a representative scan of a-type transitions. The previously unreported transitions extend the existing a-type data set to higher J (up to $J = 10$) and K_a values (up to $K_a = 2$ for all tunnelling components). The a-type transitions of all tunnelling components of $(H_2O)_2$ had previously only been

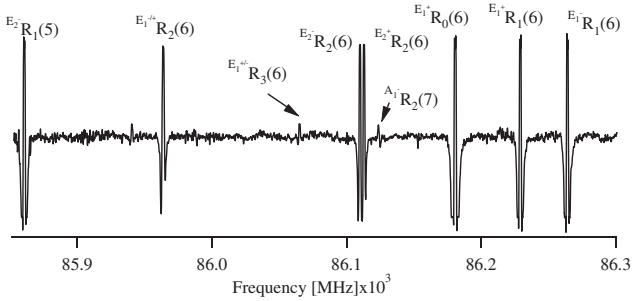

Figure 3. An experimental spectrum of a-type transitions of $(H_2O)_2$ is shown. The scan was recorded at high sensitivity, as the $K_a = 2$ and 3 transitions have very low intensity, so the higher intensity $K_a = 0$ and 1 transitions saturated the lock-in amplifier.

observed for the $K_a = 0$ level. Both previously reported and new transitions were included in the fit as no c-type transitions of the 1s of $(H_2O)_2$ were observed and also to improve the overall quality of the fit. The residuals of the E states for the $K_a = 2 \leftarrow 1$ transitions of the 2s for this fit were significantly smaller than those reported by Zwart *et al.* [18].

A total of 87 a-type ($\Delta K_a = 0$) and 23 c-type transitions of the 1s and 86 a-type and 47 c-type ($\Delta K_a = 1$) transitions of the 2s were observed and assigned for $(D_2O)_2$ and originally presented in [38]. Previously, all six tunnelling components had only been observed for $K_a = 0$ and 1, and the results from [38] extend this to $K_a = 0$–3 for all tunnelling components and the observation of E-state transitions for $K_a = 4$. Observation of c-type $K_a = 1 \leftarrow 0$ Q branch transitions of the 2s up to $J = 11$ extended the data set previously reported by Karyakin *et al.* [20], and the c-type $K_a = 2 \leftarrow 1$ data set reported by Zwart *et al.* [17] was completed by the first observation of A_2 and B_2 tunnelling components, allowing the determination of the change in bifurcation tunnelling splitting and the band origin. As pointed out previously the data here generally confirm and extend the previous results and the extension of the data set allows comparison with theory to higher K_a values. The advantage of the direct absorption technique compared to the EROS (electric resonance optothermal spectroscopy) technique is important for the E states. The EROS technique depends on the dipole moment of the states involved in the transitions and thus misses some of the E-state transitions such as the R(9) transition of $(D_2O)_2$ which it assigns to an absorption signal at 108 497.45 MHz [42]. The results presented here clearly indicate that the R(9) transition of the E_1 and E_2 states corresponds to absorption signals at 108 501.2 and 108 505.2 MHz.

All water dimer transitions were fit with the following energy expressions, typical for near prolate rotors.

Table 1. The assigned transitions of $(H_2O)_2$ reported here are shown together with the difference (Δ) between observed and calculated frequencies (all values are in MHz). The table lists the a-type transitions of the 1s. For the pair of symmetry labels, e.g. A_1^+/B_1^-, the one listed first (A_1^+) is the symmetry label of the state the transitions are originating in for all even J values and the second (B_1^-) for all odd J values. An analogous table for $(D_2O)_2$ can be found in [38].

			$K_a = 0 \leftarrow 0$			
	A_1^+/B_1^-	Δ	E_1^+/E_1^-	Δ	B_1^+/A_1^-	Δ
R(4)	84001.35	−0.28				
R(5)			73884	−0.06		
R(6)	108469.6	−0.05	86179.95	0.07		
R(7)			98467	−0.3	76275.3	−0.2
R(8)			110745	−0.12		
R(9)					101018.2	0.01
			$K_a = 1 \leftarrow 1$			
	B_1^-/A_1^+	Δ	E_1^-/E_1^+	Δ	A_1^-/B_1^+	Δ
R(1)						
R(2)						
R(3)						
R(4)	82637.25	0.28				
R(5)			73925.5	0.15		
R(6)	107133	0.48	86228.05	−0.17		
R(7)			98522.8	0.02	77661.6	−0.09
R(8)			110808.2	0.36		
R(9)					102386	0.57
	A_1^+/B_1^-	Δ	E_1^+/E_1^-	Δ	B_1^+/A_1^-	Δ
R(3)	70387.7	−0.24				
R(4)						
R(5)	94922	−0.39	73955.7	0.23		
R(6)			86263.2	−0.17		
R(7)			98562.6	−0.35		
R(8)					90111.6	0.21
R(10)					114855.8	−0.4
			$K_a = 2 \leftarrow 2$			
	B_1^-/A_1^+	Δ	E_1^-/E_1^+	Δ	A_1^-/B_1^+	Δ
R(5)	85847.7	−0.4	73697.04	0.16		
R(6)			85962.7	0.01	73834.96	0.33
R(7)	110322.8	0.12	98221	0.33		
R(8)			110469.4	−0.28	98403.2	−0.12
	A_1^+/B_1^-	Δ	E_1^+/E_1^-	Δ	B_1^+/A_1^-	Δ
R(4)	73598.3	0.36				
R(5)			73697.04	−0.18		
R(6)	98089.4	−0.06	85963.35	0.11		
R(7)			98221	−0.49	86123	−0.32
R(8)			110471.2	0.35		
R(9)					110676.6	0.14
			$K_a = 3 \leftarrow 3$			
	A_1^+/B_1^-	Δ	E_1^+/E_1^-	Δ	B_1^+/A_1^-	Δ
R(5)			73459.3	0.9		
R(6)			85684	−0.84		
R(7)			97903.2	−0.4		
R(8)			110114	0.41		

Table 2. The assigned transitions of $(H_2O)_2$ reported here are shown together with the difference (Δ) between observed and calculated frequencies (all values are in MHz). The table lists c-type transitions of the 1s. For the pair of symmetry labels, e.g. A_1^+/B_1^-, the one listed first (A_1^+) is the symmetry label of the state the transitions are originating in for all even J values and the second (B_1^-) for all odd J values. An analogous table for $(D_2O)_2$ can be found in [38].

	$K_a = 1 \leftarrow 0$					
	A_1^+/B_1^-	Δ	E_1^+/E_1^-	Δ	B_1^+/A_1^-	Δ
P(5)			367308.5[a]	−0.44		
P(4)	404054.9[a]	−0.28	379590.4[a]	−0.23		
P(3)			391883.9[a]	−0.08		
P(2)	428731.7[a]	−0.08	404187.8[a]	0.08		
Q(1)			428833.6[a]	0.03	409708.1[a]	0.1
Q(2)	453392[a]	−0.39	428857.4[a]	0.15		
Q(3)			428893[a]	0.21	409815.6[a]	0.14
Q(4)	453392.8[a]	−0.22	428940.5[a]	0.23		
Q(5)			428999.9[a]	0.28	410008.9[a]	0.26
Q(6)	453395.3[a]	0.11	429071.3[a]	0.23		
Q(7)			429154.6[a]	0.13	410287.2[a]	0.18
Q(8)	453400.3[a]	−0.18	429250.2[a]	0.01		
Q(9)			429357.8[a]	−0.32		
R(0)	465713.3[a]	−0.12	441149.6[a]	0.04		
R(1)			453482.9[a]	−0.05	434361.2[a]	0.02
R(2)	490332[a]	0.29	465820.5[a]	−0.37		
R(3)			478162.3[a]	0.25	459083.5[a]	−0.38
R(4)	514910.9[a]	0.46	490505.2[a]	−0.16		
R(5)			502849.7[a]	0.04	483844.2[a]	−0.38
R(6)	539441.2[a]	−0.05	515193.4[a]	−0.42		
R(7)			527536.9[a]	0.17	508633.2[a]	−0.09
R(8)			539877.5[a]	0.22		

[a]From Zwart *et al.* [18] and references therein.

- $K_a = 0, 3, 4$:

$$E(A^{\pm}/B^{\pm}) = \pm i^{(0)}/2 - b(0) + B^{(0)}J(J+1) - D^{(0)}(J(J+1))^2 ,$$
$$E(E^{\pm}) = b^{(0)} + B^{(0)}J(J+1) - D^{(0)}(J(J+1))^2 .$$

- $K_a = 1$:

$$\begin{aligned} E(A^{\pm}/B^{\pm}) = {} & \nu^{(1)} \pm i^{(1)}/2 - b^{(1)} + B^{(1)}(J(J+1)-1) \\ & - D^{(1)}(J(J+1)-1)^2 \pm ((B-C)^{(1)}/4 \\ & - d^{(1)}J(J+1))J(J+1) , \\ E(E^{\pm}) = {} & \nu^{(1)} + b^{(1)} + B^{(1)}(J(J+1)-1) \\ & - D^{(1)}(J(J+1)-1)^2 \pm ((B-C)^{(1)}/4 \\ & - d^{(1)}J(J+1))J(J+1) . \end{aligned}$$

- $K_a = 2$:

$$\begin{aligned} E(A\pm/B\pm) = {} & \nu^{(2)} \pm i^{(2)}/2 - b^{(2)} + B^{(2)}(J(J+1)-4) \\ & - D^{(2)}(J(J+1)-4)^2 \pm (c^{(2)}/4)J(J+1) \\ & \times (J-1)(J+2) , \\ E(E^{\pm}) = {} & \nu^{(2)} + b^{(2)} + B^{(2)}(J(J+1)-4) \\ & - D^{(2)}(J(J+1)-4)^2 \pm (c^{(2)}/4)J(J+1) \\ & \times (J-1)(J+2), \end{aligned}$$

where $\nu^{(n)}$ is the band origin of the $K_a = n$ levels; $i^{(n)}$ is the interchange tunnelling splitting in $K_a = n$; $b^{(n)}$ is the bifurcation tunnelling splitting in $K_a = n$; $B^{(n)}$ is the average of the B and C rotational constants in $K_a = n$; $D^{(n)}$ is the D (distortion) rotational constant in $K_a = n$; $d^{(1)}$ is the d (distortion) rotational constant in $K_a = 1$ and $c^{(2)}$ is the asymmetry splitting constant for $K_a = 2$.

The energy level expression for those states affected by the Coriolis perturbation mentioned in section 2 is

$$E = [E^{(0)} + E^{(1)}]/2 \pm [(E^{(1)} - E^{(0)})_2/4 + \zeta^2 J(J+1)/2]^{1/2} ,$$

where the $E^{(n)}$ are the conventional unperturbed energy levels given above and ζ is the Coriolis interaction constant. For the fits reported here, the values of ζ were fixed to the previously determined values [24] as they could not be fit without high correlation.

The molecular constants determined in the fits, shown in tables 5 and 6, and the tunnelling splittings, shown in tables 7 and 8, agree well with those previously reported. The study allows the quantification of rotational constants and tunnelling splittings for a number of previously unobserved rotation-tunnelling states. This, in turn, allows the calculation of combination differences which will aid in assigning vibration–rotation tunnelling (VRT) transitions originating (and terminating) in large K_a states of $(D_2O)_2$ and especially of $(H_2O)_2$. Furthermore, these transitions are presently being incorporated into the fit of a new version of the VRT(ASP-W) potential to the experimental data.

4.1. *Rotational constants*

The B rotational constant decreases with increasing K_a for both isotopomers, as no D_{JK} or D_K distortion constants were included in the fits. The only exceptions are the $K_a = 1$ levels, in which the $B^{(1)}$ rotational constants of the 1s show a slight increase compared to $K_a = 0$ for both isotopomers. The observation of large K_a values allows an estimate of both D_{JK} and D_K although these results (especially for D_K) have to be regarded with caution due to the extensive coupling of the overall rotation with tunnelling. D_{JK} can be estimated from the E-state constants of $K_a = 0$, 2 and 3 using the expression $B^{(K_a)} = B - D_{JK}K_a^2$. From this, a value of $D_{JK} = 4.03/2.84$ and $1.77/1.17$ MHz can be

Table 3. The assigned transitions of $(H_2O)_2$ reported here are shown together with the difference (Δ) between observed and calculated frequencies (all values are in MHz). The table lists the a-type transitions of the 2s. For the pair of symmetry labels, e.g. A_1^+/B_1^-, the one listed first (A_1^+) is the symmetry label of the state the transitions are originating in for all even J values and the second (B_1^-) for all odd J values. An analogous table for $(D_2O)_2$ can be found in [38].

			$K_a = 0 \leftarrow 0$			
	A_2^-/B_2^+	Δ	E_2^-/E_2^+	Δ	B_2^-/A_2^+	Δ
R(0)	31673.4[a]	−0.11				
R(1)	43797.03[a]	−0.08	24284.32[a]	−0.03		
R(2)	55916.67[a]	−0.21	36464.94[a]	−0.01	17122.62[a]	−0.28
R(3)	68043.3	−0.44	48675.12[a]	−0.02	29416.39[a]	−0.28
R(4)	80182.5	−0.35			41734.73[a]	−0.27
R(5)	92334.4	−0.22	73160.8	0.15	54068.53[a]	−0.24
R(6)	104496.4	−0.19	85422.1	0.23	66410.42	−0.32
R(7)	116665	0.05	97687.2	−0.28	78755.73	0.15
R(8)			109953	0.03	91099.7	0.2
R(9)					103439.8	−0.01
R(10)					115774.4	−0.05
			$K_a = 1 \leftarrow 1$			
	B_1^+/A_1^-	Δ	E_1^+/E_1^-	Δ	A_1^+/B_1^-	Δ
R(1)			24548.3[a]	−0.14	8344.46[a]	−0.17
R(2)	53015.86[a]	−0.54	36819.84[a]	0.01	20620.65[a]	−0.11
R(3)	65275.95[a]	−0.62	49087.38[a]	−0.44	32895.28[a]	−0.29
R(4)	77529	−0.97			45167.86[a]	−0.1
R(5)	89775	−0.36	73609.16	0.09	57436.73[a]	−0.1
R(6)	102011.6	0.06	85860.15	0.09	69701.5	0.38
R(7)	114238	0.76	98102.8	−0.32	81959.55	−0.22
R(8)			110336.84	−0.28	94211.8	0.06
R(9)					106456.2	0.21
	A_1^-/B_1^+	Δ	E_1^-/E_1^+	Δ	B_1^-/A_1^+	Δ
R(1)			25048.44[a]	0.15	8756.58[a]	0.01
R(2)	53753.29[a]	−0.58	37528.94[a]	0.78	21189.82[a]	−0.01
R(3)	66233.2[a]	−0.85	49971.38[a]	−0.06	33594.83[a]	−0.01
R(4)	78678.6	−0.92			45978.83[a]	−0.06
R(5)	91086.8	−0.75	74762.4	−0.09		
R(6)	103458	−0.31	87119.55	−0.15	70708.9	−0.15
R(7)	115793.6	0.25	99456	−0.17	83062.95	0.08
R(8)					95411.5	0.01
R(10)					107755.2	0.03
			$K_a = 2 \leftarrow 2$			
	B_1^+/A_1^-	Δ	E_1^+/E_1^-	Δ	A_1^+/B_1^-	Δ
R(4)	72584.19	−2.06				
R(5)	84863.2	−1.01	73825.84	0.06		
R(6)	97131.8	−0.24	86112.2	0	75096	−0.36
R(7)	109388.4	−0.16	98390.4	0.05	87393.8	−0.49
R(8)			110659.4	0.32	99684.8	−0.06
R(9)					111967.1	0.34

continued

Table 3. (*continued*)

	A_1^-/B_1^+	Δ	E_1^-/E_1^+	Δ	B_1^-/A_1^+	Δ
R(4)	72585.49	−1.57				
R(5)	84864.8	−0.75	73824.04	0.1		
R(6)	97134	−0.06	86109.2	−0.05	75099.8	−0.35
R(7)	109391.6	0.2	98386	0.06	87399.6	−0.56
R(8)			110653.1	0.32	99693.2	−0.31
R(9)					111979.1	0.06
			$K_a = 3 \leftarrow 3$			
	A_1^+/B_1^-	Δ	E_1^+/E_1^-	Δ	B_1^+/A_1^-	Δ
R(5)			73784.88	0.06		
R(6)			86064.45	0.08		
R(7)			98335.4	−0.25		
R(8)			110597.6	0.12		

[a]From Zwart *et al.* [18] and references therein.

Table 4. The assigned transitions of $(H_2O)_2$ reported here are shown together with the difference (Δ) between observed and calculated frequencies (all values are in MHz). The table lists the a-type transitions of the 2s. For the pair of symmetry labels, e.g. A_1^+/B_1^-, the one listed first (A_1^+) is the symmetry label of the state the transitions are originating in for all even J values and the second (B_1^-) for all odd J values. An analogous table for $(D_2O)_2$ can be found in [38].

			$K_a = 1 \leftarrow 0$			
	A_1^-/B_1^+	Δ	E_1^-/E_1^+	Δ	B_1^-/A_1^+	Δ
P(6)	−36804.25[a]	−0.01				
P(5)	−25899.06[a]	0.14				
P(4)	−14826.98[a]	0	−35286.6[a]	0.02		
P(3)			−24139.64[a]	0.01		
Q(1)	32112.47[a]	0.17				
Q(2)	32297.22[a]	0.05				
Q(3)	32553.28[a]	−0.04				
Q(4)	32860.8[a]	−0.16				
Q(5)	33199.97[a]	−0.15				
Q(6)	33552.54[a]	−0.12				
Q(7)	33903.33[a]	0.2				
R(1)			36609.62[a]	−0.03	21616.23[a]	0.14
R(2)					34768.42[a]	0.03
R(3)	83880.17	0.63				
R(5)					75613.1	−0.11
R(6)	111166.97	−0.26			89541.2	−0.46
R(7)					103569	−0.03
R(8)					117670.8	−0.02

continued

Table 4. (*continued*)

	$K_a = 2 \leftarrow 1$					
	B_2^+/A_2^-	Δ	E_2^+/E_2^-	Δ	A_2^+/B_2^-	Δ
P(5)	610301.8[a]	−1.6				
P(4)	622426.4[a]	−1.49				
P(3)	634590[a]	−1.51			607318[a]	−0.74
Q(2)			660538[a]	−0.63	644133.3[a]	−0.96
Q(3)	671519.8[a]	1.4	660648.3[a]	0.69	644253[a]	−1.16
Q(4)	671659.4[a]	1.03	660793.4[a]	0.7	644412.4[a]	−1.49
Q(5)	671832.6[a]	−0.39	660973.7[a]	−0.02	644611.4[a]	−1.92
Q(6)	672042.4[a]	0.36	661190.4[a]	−0.03		
Q(7)			661442.3[a]	−0.27		
Q(8)			661729.7[a]	−0.1		
R(1)	695963.1[a]	0.17	685087.1[a]	0.08	668681.7[a]	1.93
R(2)	708339.2[a]	−0.67	697466.8[a]	−0.37	681070[a]	0.66
R(3)	720749.1[a]	1.17			693494.4[a]	−0.52
R(4)	733185.6[a]	0.01			705953.9[a]	−1.11
R(5)	745652.1[a]	0.84			718448.9[a]	0.89
R(6)	758144[a]	0.78			730972.8[a]	0.54
R(7)					743526.1[a]	0.13
R(8)			772371.[a]	−0.05		
	A_1^-/B_1^+	Δ	E_1^-/E_1^+	Δ	B_1^-/A_1^+	Δ
P(5)	607247.3[a]	−1.54				
P(4)					592927.3[a]	−0.64
P(3)	633305.1[a]	0.41				
Q(2)	670757.1[a]	0.36	659778.9[a]	0.05	643415.8[a]	−0.6
Q(3)	670232.4[a]	1.11	659178.7[a]	−0.58	642859.2[a]	−0.74
Q(4)	669565.3[a]	0.85	658440.1[a]	−0.12	642167.6[a]	−1.1
Q(5)	668777.2[a]	1.14	657590.8[a]	0.57	641367[a]	−1.59
Q(6)	667883.5[a]	−0.62	656652.2[a]	0.52	640478.9[a]	−2
Q(7)	666904.4[a]	0.51	655640.8[a]	−0.43		
Q(8)			654570.9[a]	−0.11		
R(1)	695741.2[a]	0.23	684827[a]	−0.19	668437.5[a]	2.21
R(2)	707684[a]	0.37	696708[a]	0.29	680351.9[a]	0.08
R(3)	719463[a]	1.23			692100.3[a]	−1.52
R(4)	731095[a]	0.95			703712.5[a]	−0.14
R(5)	742598.5[a]	−0.8			715212.8[a]	3.6
R(6)					726612.7[a]	0.8
R(7)	765293.9[a]	−0.36			737936[a]	−0.43

[a]From Zwart *et al*. [18] and references therein.

determined for the 1s/2s of H_2O and 1s/2s of D_2O, respectively, in agreement with a larger decrease of $B^{(K_a)}$ with increasing K_a for $(H_2O)_2$. The $A^{(1)}$ rotational constants agree well with those determined by Zwart *et al*. [18] for $(H_2O)_2$ and Karyakin *et al*. [20] for $(D_2O)_2$, but the $A^{(2)}$ rotational constant determined by Zwart *et al*. [17] for $(D_2O)_2$ is *ca*. 300 MHz larger, probably because the authors did not observe all tunnelling components of the 2s and thus could not determine the band origin rigorously. It is also possible to estimate a K_a-independent, A rotational constant = 124 717 MHz and D_K distortion constant = −207 MHz for $(D_2O)_2$ in a similar way to the estimate of D_{JK}, but using the expression $A^{(K_a)} = A - D_K K_a^2$.

4.2 *Tunnelling splittings*

The only tunnelling splitting that can be directly determined from experiment is for interchange. The

Table 5. The rotational constants determined for $(H_2O)_2$ in the fit are shown (all values in MHz). The $A^{(1)}$-rotational constant was determined from the band origins of $K_a = 1$ and $A^{(1)} = [\nu^{(1)}(1s) + \nu^{(1)}(2s)]/2$.

		A_1^+/B_1^-	E_1^+/E_1^-	B_1^+/A_1^-	A_2^-/B_2^+	E_2^-/E_2^+	B_2^-/A_2^+
$K_a = 0$	$B^{(0)}$	6163.921 (27)	6160.604 (19)	6158.292 (31)	6167.736 (26)	6166.652 (53)	6164.746 (36)
	$D^{(0)}$	0.05043 (26)	0.04998 (17)	0.04924 (41)	0.03824 (29)	0.03649 (52)	0.03788 (49)
$K_a = 1$	$A^{(1)}$			227575.33 (60)			
	$\nu^{(1)}$		436345.53 (12)			18805.14 (84)	
	$B^{(1)}$	6167.167 (22)	6165.165 (18)	6162.207 (27)	6153.433 (20)	6152.279 (38)	6151.129 (24)
	$D^{(1)}$	0.04981 (21)	0.04949 (16)	0.04895 (30)	0.05396 (20)	0.05403 (38)	0.05419 (31)
	$d^{(1)}$	0[b]	0[b]	0[b]	0.00631 (13)	0.00682 (27)	0.00594 (21)
	ζ	0[b]	0[b]	0[b]	1594.100[b]	1508.674[b]	1538.377[b]
	$(B\text{-}C)^{(1)}/4$	1.7810 (28)	1.2550 (21)	1.6230 (31)	15.7321 (79)	14.899 (16)	14.459 (10)
$K_a = 2$	$\nu^{(2)}$					697814.12 (65)	
	$B^{(2)}$	6145.064 (46)[a]	6144.395 (32)[a]	6142.692 (99)[a]	6156.382 (20)	6155.286 (38)	6154.963 (26)
	$D^{(2)}$	0.04382 (40)[a]	0.04648 (26)[a]	0.03884 (90)[a]	0.05068 (21)	0.05023 (34)	0.05052 (32)
	$c^{(2)}$	0[b]	0.000203 (69)[a]	0[b]	0.001174 (56)	0.001094 (73)	0.000986 (73)
$K_a = 3$	$B^{(3)}$		6124.457 (45)[a]			6151.886 (92)	
	$D^{(3)}$		0.04569 (37)[a]			0.04923 (76)	

1σ uncertainties of fitted constants in parentheses.
[a] Previously not reported molecular constants; RMS: 0.30 MHz (1s), 0.69 MHz (2s).
[b] Fixed.

Table 6. The rotational constants determined for $(D_2O)_2$ in the fit are shown (all values in MHz). They agree well with those previously determined although $B^{(1)}$ and $B^{(2)}$ are about 0.1 MHz smaller. The $A(K_a)$-rotational constants were determined from the band origins of the $K_a = 1$ (for $A^{(1)}$) and $K_a = 2$ (for $A^{(2)}$) transitions, and e.g. $A^{(1)} = [\nu^{(1)}(1s) + \nu^{(1)}(2s)]/2$.

		A_1^+/B_1^-	E_1^+/E_1^-	B_1^+/A_1^-	A_2^-/B_2^+	E_2^-/E_2^+	B_2^-/A_2^+
$K_a = 0$	$B^{(0)}$	5432.597 (7)	5432.331 (7)	5432.139 (8)	5432.518 (14)	5432.409 (18)	5432.215 (16)
	$D^{(0)}$	0.03655 (5)	0.03635 (5)	0.03634 (5)	0.03534 (9)	0.03572 (11)	0.03535 (11)
$K_a = 1$	$A^{(1)}$			124923.74 (23)			
	$\nu^{(1)}$		160696.53 (12)			89150.95 (11)	
	$B^{(1)}$	5433.027 (6)	5432.850 (5)	5432.683 (5)	5430.509 (56)	5430.427 (17)	5430.239 (15)
	$D^{(1)}$	0.03566 (4)	0.03552 (4)	0.03566 (4)	0.03523 (9)	0.03545 (11)	0.03513 (10)
	$(B\text{-}C)^{(1)}/4$	8.2773 (13)	8.2799 (17)	8.2562 (13)	14.9073 (31)	14.8605 (50)	14.8167 (31)
$K_a = 2$	$A^{(2)}$			125545.3 (2.3)			
	$\nu^{(2)}$		548296.62 (49)			456066.1 (1.6)	
	$B^{(2)}$	5425.280 (11)	5425.223 (10)	5425.194 (8)	5427.865 (25)[a]	5427.823 (20)	5427.746 (18)[a]
	$D^{(2)}$	0.03439 (7)	0.03445 (6)	0.03445 (5)	0.03536 (17)[a]	0.03562 (14)	0.03541 (13)[a]
	$(B\text{-}C)^{(2)}/4$	0.000231 (8)	0.00023 (1)	0.000240 (8)	0.00086 (3)[a]	0.00084 (4)	0.00085 (3)[a]
$K_a = 3$	$B^{(3)}$	5416.477 (19)[a]	5416.549 (15)[a]	5416.586 (14)[a]	5421.613 (38)[a]	5421.671 (29)[a]	5421.582 (38)[a]
	$D^{(3)}$	0.03444 (13)[a]	0.03444 (10)[a]	0.03447 (10)[a]	0.03482 (25)[a]	0.03490 (20)[a]	0.03438 (26)[a]
$K_a = 4$	$B^{(4)}$		5411.97 (3)[a,b]			5412.63 (3)[a,b]	

1σ uncertainties of fitted constants in parentheses.
[a] Recently reported molecular constants [38]; RMS: 0.24 MHz (1s), 0.38 MHz (2s), 0.8M Hz ($K_a = 4$ values 1s, 2s).
[b] Tentative assignment (only 3 transitions observed for 1s and 2s).

experimentally determined interchange tunnelling splittings decrease with increasing K_a for both $(H_2O)_2$ and $(D_2O)_2$, with this tunnelling splitting being *ca.* 20 times larger in $(H_2O)_2$. The relative decrease with K_a is larger for $(H_2O)_2$ than $(D_2O)_2$ and larger for the 1s than the 2s for both isotopomers. The results presented here agree well with previous results and significantly extend the K_a states for which this tunnelling splitting has been characterized ($K_a = 2$–3).

Only the difference in the magnitude of the acceptor switching splitting can be determined experimentally. As the order of the 1s and 2s is reversed for $K_a = 1$, this

Table 7. Calculated dissociation energies and experimental and calculated tunnelling splittings for $(H_2O)_2$ are shown. The difference between experimental and calculated values is shown in parentheses. All values are in cm^{-1}. The superscripts refer to the K_a value and the subscript to either the 1s or 2s. Only the interchange tunnelling splitting, $i^{(n)}$, can be determined directly in the experiment. Therefore, the calculated acceptor and bifurcation tunnelling splittings $a^{(n)}$ and $b^{(n)}$ are shown along with the experimentally determined sums e.g. $a^{(01)}$ and $b^{(01)}$. These are defined as follows:

$$a^{01} = \nu_{B_1^-\rightarrow B_1^+/A_1^-} + 2\nu_{E_1\rightarrow E_1} + \nu_{A_1^-\rightarrow A_1^+/B_1^-} - \left[\nu_{B_2^+\rightarrow B_2^-/A_2^+} + 2\nu_{E_2\rightarrow E_2} + \nu_{A_2^+\rightarrow A_2^-/B_2^+}\right],$$

for ${}^RQ_0(1)$ transitions to the average of the $K_a = 1$ asymmetry doublets. This is equivalent to $a^{01} = |a^0| + |a^1|$ given as the definition in section 4.2 for the experimental values. $b_1^{01} = (b_1^0 - b_1^1)/2$. Analogous expressions were used for the 2s.

K_a		Experiment[a]	VRT(ASP-W)III[a]	SAPT-5st[a]	VRT(MCY-5f)[b]
0	a^0	9.34[c]	10.831	11.021	11.725
	a^{01}	13.919	13.662 (2%)	13.510 (3%)	13.807 (1%)
	$i_1{}^0$	0.752368 (17)	0.334 (56%)	0.762 (1%)	0.602 (20%)
	$i_2{}^0$	0.651481 (13)	0.359 (45%)	0.683 (5%)	0.609 (7%)
	$b_1{}^0$	Unknown	0.319	0.021	0.116
	$b_2{}^0$	Unknown	0.312	0.019	−0.004
	$b_1{}^{01}$	0.022659 (2)	0.310 (1300%)	0.020 (12%)	0.054 (140%)
	$b_2{}^{01}$	0.024906 (7)	0.301 (1100%)	0.022 (12%)	0.059 (140%)
1	a^1	Unknown	−2.831	−2.493	−2.087
	$i_1{}^1$	0.705335 (15)	0.308 (56%)	0.746 (6%)	0.602 (15%)
	$i_2{}^1$	0.540535 (11)	0.266 (51%)	0.560 (4%)	0.465 (14%)
	$b_1{}^1$	Unknown	−0.301	−0.019	0.008
	$b_2{}^1$	Unknown	−0.289	−0.024	−0.121
	$b_2{}^{12}$	−0.023073 (3)	−0.288 (1100%)	−0.021 (9%)	−0.050 (120%)
2	a^2	Unknown	−8.66	−8.60	−9.799
	$i_1{}^2$	0.407715 (33)	0.220 (46%)	0.508 (25%)	0.454 (11%)
	$i_2{}^2$	0.369619 (15)	0.154 (58%)	0.415 (12%)	0.323 (13%)
	$b_1{}^2$	Unknown	0.281	0.017	0.145
	$b_2{}^2$	Unknown	0.287	0.017	−0.022
Calc. Energy of $J=0$, $K_a=0$ A_1^+			1074.85	1075.27	1232.26

[a]As determined in a fit to $a^{(K_a)} = \cos[2\pi K_a/3.0] \times 280\,\text{GHz}$.
[b]From Leforestier [46].
[c]This work.

corresponds to the sum of the absolute values of the acceptor switching splitting in $K_a = 0$ and 1 ($a^{01} = |a^0| + |a^1|$, see table 7 and figure 2). Paul *et al.* [23] determined a value of $a^0 = 53\,\text{GHz}$ for $K_a = 0$ of $(D_2O)_2$ by fitting data to a functional form for the acceptor switching splitting $a^{(K_a)} = \cos(2\pi K_a/3.2) \times 53\,\text{GHz}$. A similar fit for $(H_2O)_2$ assuming a fixed A rotational constant and a symmetric acceptor switching splitting gives $a^{(K_a)} = \cos[2\pi K_a/3.0] \times 280\,\text{GHz}$, which predicts a $K_a = 0$ acceptor switching splitting of 280 GHz or $9.34\,cm^{-1}$. The limitations of this approach will be discussed below, in section 4.3.

As with the acceptor switching splitting, only the change in bifurcation tunnelling splitting can be directly determined from the experimental data. Theory predicts that the sign of b alternates with K_a, and thus the sum of the absolute values of the bifurcation tunnelling splittings can be determined from experiment ($2b^{01} = |b^0| + |b^1|$, see table 7 and figure 2). The change of the bifurcation tunnelling splitting is not known, but can be estimated from tables 7 and 8; the absolute value decreases slightly, decreasing with increasing K_a.

4.3. *Comparison with theory*

The VRT(ASP-W)III [26], SAPT-5st [7, 43–45] and VRT(MCY-5f) [8] potentials were chosen as the most suitable dimer potentials for calculations of the dimer rotation-tunnelling states. These potentials have been described in detail elsewhere. All calculations were performed using the pseudospectral split-Hamiltonian approach (PSSH) [21, 26, 38] except for VRT(MCY-5f) which was taken from Leforestier [46]. The radial range was 4.5–6.5 bohr units, using 16 radial functions with 19

Table 8. Calculated dissociation energies and experimental and calculated tunnelling splittings for $(D_2O)_2$ are shown. All values are in cm^{-1}. The definitions are analogous to those given in table 4.

K_a		Experiment	VRT(ASP-W)III	SAPT-5st
0	a^0	1.768[a]	1.592	1.68
	a^{01}	2.387	2.12 (11%)	2.199 (8%)
	${i_1}^0$	0.039	0.016 (59%)	0.043 (10%)
	${i_2}^0$	0.036	0.016 (56%)	0.041 (14%)
	${b_1}^0$	Unknown	0.020	−0.006
	${b_2}^0$	Unknown	0.018	−0.004
	${b_1}^{01}$	2.4×10^{-4}	0.020 (8200%)	−0.006 (2400%)
	${b_2}^{01}$	2.4×10^{-4}	0.019 (7800%)	−0.005 (2000%)
1	a^1	−0.619[a]	−0.520	−0.524
	a^{12}	0.689	0.650 (6%)	0.696 (1%)
	${i_1}^1$	0.036	0.015 (58%)	0.041 (14%)
	${i_2}^1$	0.033	0.015 (55%)	0.038 (15%)
	${b_1}^1$	Unknown	−0.019	0.005
	${b_2}^1$	Unknown	−0.019	0.005
	${b_1}^{12}$	-2.0×10^{-4}	−0.018 (8900%)	0.004 (1600%)
	${b_2}^{12}$	-2.2×10^{-4}	−0.019 (8500%)	0.005 (2200%)
2	a^2	−1.309[a]	−1.177	−1.220
	${i_1}^2$	0.027	0.013 (52%)	0.033 (22%)
	${i_2}^2$	0.027	0.012 (56%)	0.032 (19%)
	${b_1}^2$	Unknown	0.017	−0.003
	${b_2}^2$	Unknown	0.019	−0.006
3	a^3	Unknown	1.223	1.167
	${i_1}^3$	0.018	0.009 (50%)	0.023 (28%)
	${i_2}^3$	0.020	0.003 (85%)	0.026 (30%)
	${b_1}^3$	Unknown	−0.015	0.007
	${b_2}^3$	Unknown	−0.024	0.004
Calc. Energy of $J=0$, $K_a=0$ A_1^+		1214.23	1221.57	

[a]As determined from the a^0 value of Paul *et al.* (Ref. 23) in a fit to $a^{(Ka)} = \cos(2\pi K_a/3.2) \times 53\,\mathrm{GHz}$.

radial points, four of which were kept after HEG contraction [47] and $j_{max} = 11$. This was determined as a sufficient basis size with a reasonable calculation time. The calculated dissociation energy (D_e) of $(H_2O)_2$, as judged by the $J = 0$, $K_a = 0$ A_1^+ level, was $1074.85\,cm^{-1}$ for VRT(ASP-W)III, $1075.27\,cm^{-1}$ for SAPT-5st and $1232.26\,cm^{-1}$ for VRT(MCY-5f). The calculated dissociation energies (D_e) of $(D_2O)_2$ were $1214.23\,cm^{-1}$ for VRT(ASP-W)III and $1221.57\,cm^{-1}$ for SAPT-5st. The $(H_2O)_2$ dissociation energy calculated with VRT(MCY-5f) is significantly higher than those of the other two potentials, and is even higher than the binding energy of $(D_2O)_2$ calculated with VRT(ASP-W)III and SAPT-5st. This is expected because of the inclusion of monomer relaxation in VRT(MCY-5f). A larger dissociation energy results in a larger equilibrium constant (K_p) of dimerization, which implies that current calculations, using rigid monomer potentials [32] are expected to underestimate the atmospheric water dimer concentrations.

Table 7 for $(H_2O)_2$ and table 8 for $(D_2O)_2$ show that the interchange splitting calculated on the VRT(ASP-W)III potential is systematically more than 50% too small for all K_a values of both isotopomers. It is remarkable that the interchange splitting of the earlier VRT(ASP-W)II potential agrees much better with the experimental results. The main difference between the two VRT(ASP-W) potentials is the inclusion of a few additional transitions in the fit. The results calculated with SAPT-5st agree very well with experiment for both $(H_2O)_2$ and $(D_2O)_2$. The SAPT-5st interchange splittings are always slightly too large, and this difference gets larger with increasing K_a for both isotopomers, but is always within 30%. The interchange splitting calculated on VRT(MCY-5f) gives interchange splittings that are slightly too small. It agrees better with experiment than VRT(ASP-W)III, but worse than SAPT-5st, except for $K_a = 2$. All potentials reproduce the observed decrease of the interchange splitting with K_a.

The calculated value for a^{01} of $(H_2O)_2$ agrees well with experiment for all potentials, with VRT(MCY-5f) showing the best agreement. For $(D_2O)_2$, SAPT-5st agrees better with experiment than VRT(ASP-W)III for both a^{01} and a^{12}, but agreement is good for both

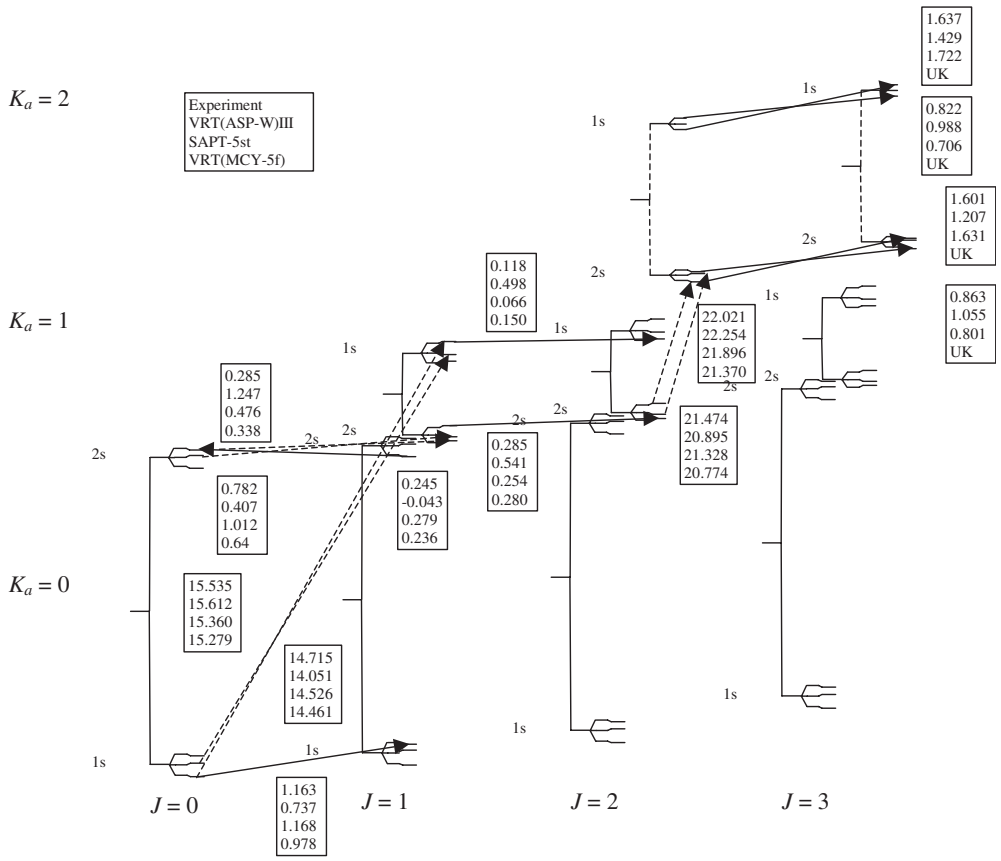

Figure 4. A comparison of $(H_2O)_2$ transitions calculated from the experimental fit and the theoretical results in cm^{-1}. The acceptor switching and interchange tunnelling splittings are drawn to scale according to the experimental results. The a-type transitions are shown as solid arrows and the c-type transitions as dashed arrows.

potentials. The estimated experimental a^n values discussed in section 4.2 for both $(D_2O)_2$ and especially $(H_2O)_2$ have much poorer agreement with the experimental ones than do the a^{01} and a^{12} values, indicating the limitations of the method described for estimating them.

The worst relative agreement is observed for the bifurcation tunnelling splittings of $(D_2O)_2$ which is not surprising, as these are very small ($\sim 2.4 \times 10^{-4}\,cm^{-1}$) and beyond the precision of the calculations. The bifurcation tunnelling splittings calculated with VRT(ASP-W)III are more than ten times too large for $(H_2O)_2$ and nearly one hundred times too large for $(D_2O)_2$. This makes the bifurcation splitting comparable to the interchange splitting for VRT(ASP-W)III. SAPT-5st reproduces the experimental $(H_2O)_2$ results with remarkable quality while slightly under-predicting the magnitude of the bifurcation splitting. The SAPT-5st $(D_2O)_2$ bifurcation splittings have the opposite sign of the experimental ones and their magnitude is significantly too large. VRT(MCY-5f) gives bifurcation tunnelling splittings that are too large by *ca.* a factor of two. It is worth noting that the SAPT-5st potential was determined by tuning it with respect to $(H_2O)_2$ data, and perhaps this explains the poorer agreement for $(D_2O)_2$.

Figures 4 and 5 show that the observed and calculated transitions also agree best for the SAPT-5st potential. The agreement of observed transitions with those calculated on VRT(ASP-W)III is worse (see figures 4 and 5), which results mainly from the poor values of interchange and bifurcation tunnelling splitting. Only $(H_2O)_2$ results were available for the VRT(MCY-5f) potential which generally shows good agreement with experiment—in between the SAPT-5st and the VRT(ASP-W)III potentials. The only transitions that do not agree well for the VRT(MCY-5f) potential are the $K_a = 2 \leftarrow 1$ transitions.

5. Conclusions

The results presented in this paper extend the existing water dimer data set to larger J and K_a values. The transitions probe the dimer intermolecular potential energy surface up to energies of *ca.* $70\,cm^{-1}$ ($K_a = 4$) for $(D_2O)_2$ and *ca.* $80\,cm^{-1}$ ($K_a = 3$) for $(H_2O)_2$. These energies are comparable to low-lying intermolecular vibrations and thus represent an additional test of the

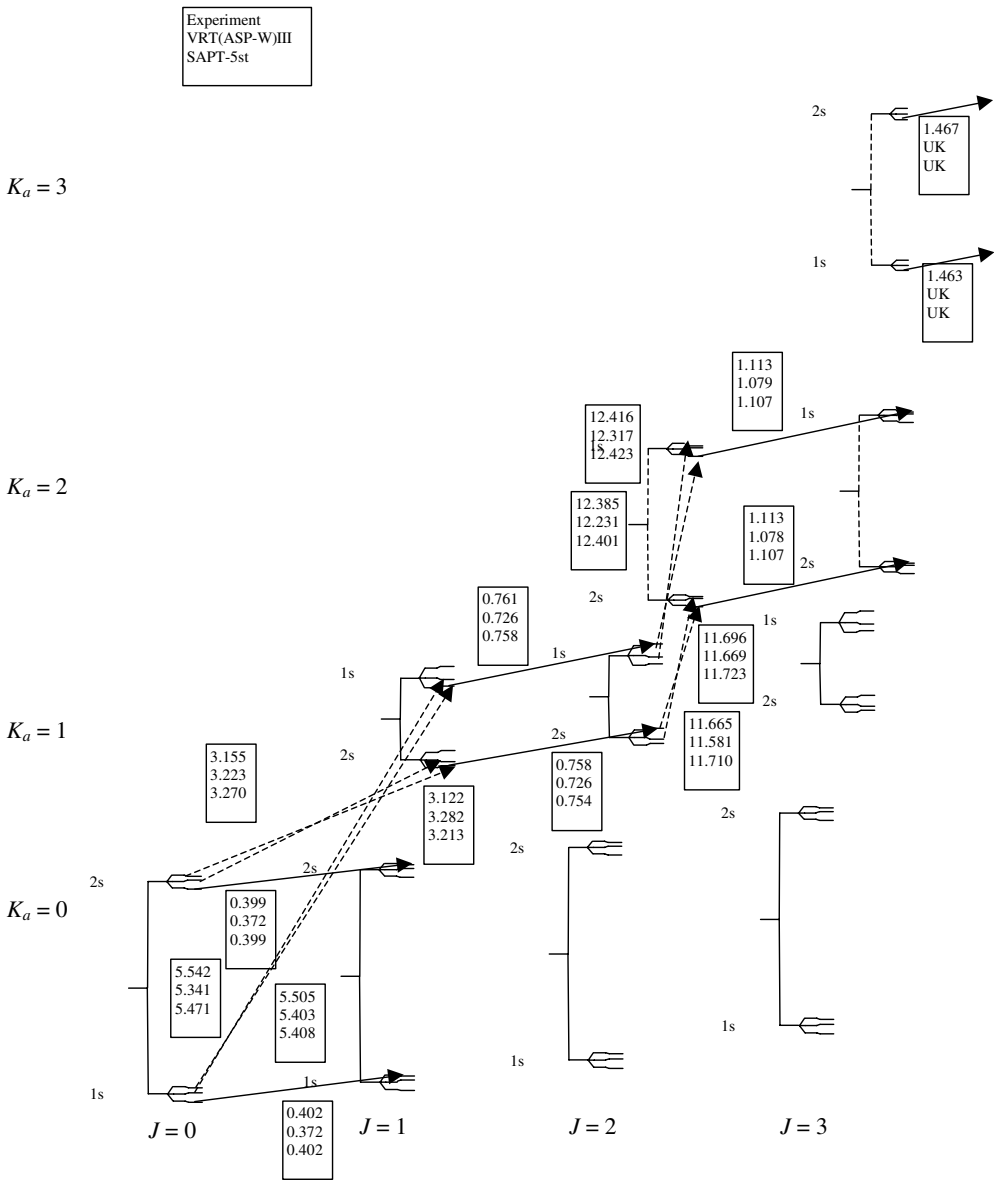

Figure 5. A comparison of $(D_2O)_2$ transitions calculated from the experimental fit and the theoretical results. The acceptor switching and interchange tunnelling splittings are drawn to scale according to the experimental results. The a-type transitions are shown as solid arrows and the c-type transitions as dashed arrows.

intermolecular potential energy surface at these energies. VRT(MCY-5f) produces the best agreement with experiment for the intermolecular vibrations, with VRT(ASP-W)III and SAPT-5st being comparable [27]. In contrast, SAPT-5st clearly produces the best agreement with experiment for the pure rotation-tunnelling states, with VRT(MCY-5f) being slightly worse and VRT(ASP-W)III yielding rather poor agreement. SAPT-5st was formed from 'tuning' of a very good *ab initio* potential, which could explain this better agreement. The poorer agreement of VRT(MCY-5f) may result from the fact that the MCY functional form [48] has a very simple form. VRT(ASP-W)III was determined in a fit to $(D_2O)_2$ data, which has much smaller tunnelling splittings, especially for bifurcation. Thus, it is possible that the bifurcation tunnelling splitting does not get reproduced well by VRT(ASP-W)III. It is also remarkable that the sum of interchange and bifurcation tunnelling is close to the experimental interchange tunnelling. Possibly, this arises from the details of the transitions used in the fit of the VRT(ASP-W)III potential. This also indicates that the initial VRT(ASP-W) potential needs to be constrained by a prudent choice of parameters or that a potential fit to $(D_2O)_2$ does not necessarily give good $(H_2O)_2$ results (although the trends in agreement with experiment are

similar for both isotopomers). While the absolute errors are not very large (as, for example, the bifurcation tunnelling splitting is very small), the magnitude of the errors is an important quality test for any model IPS as these tunnelling splittings probe the entire potential energy surface. Our conclusion of this study, as well as the previous one on the intermolecular vibrational states, is that all three potentials are good candidates for a 'universal' water potential. The SAPT-5st potential and also the VRT(MCY-5f) potential are excellent candidates for accurate water dimer potentials to be utilized in highly accurate and precise calculations for water dimer equilibrium concentrations. However, since these models do not contain explicit tensorial polarizability, they cannot produce the many-body induction that is so important in condensed phase interactions. It should be emphasized that because VRT(MCY-5f) explicitly takes coupling between inter- and intramolecular vibrations into account, this makes it ideally suited for calculations of intramolecular spectra (e.g. the overtone spectra used by Pfeilsticker *et al.* [33] in their atmospheric observations).

This work was supported by the Experimental Physical Chemistry program of the National Science Foundation.

References

[1] Marshall, M. D., Charo, A., Leung, H., and Klemperer, W., 1985, *J. chem. Phys.*, **83,** 4924.

[2] Nelson, D. D., Fraser, G. T., and Klemperer, W., 1987, *Science*, **238,** 1670.

[3] Cohen, R. C., Busarow, K. L., Laughlin, K. B., Blake, G. A., Havenith, M., Lee, Y. T., and Saykally, R. J., 1988, *J. chem. Phys.*, **89,** 4494.

[4] Saykally, R. J., and Blake, G. A., 1993, *Science*, **259,** 1570.

[5] Elrod, M. J., and Saykally, R. J., 1995, *J. chem. Phys.*, **103,** 933.

[6] Fellers, R. S., Leforestier, C., Braly, L. B., Brown, M. G., and Saykally, R. J., 1999, *Science*, **284,** 945.

[7] Groenenboom, G. C., Mas, E. M., Bukowski, R., Szalewicz, K., Wormer, P. E. S., and van der Avoird, A., 2000, *Phys. Rev. Lett.*, **84,** 4072.

[8] Leforestier, C., Gatti, F., Fellers, R. S., and Saykally, R. J., 2002, *J. chem. Phys.*, **117,** 8710.

[9] Keutsch, F. N., and Saykally, R. J., 2001, *Proc. Natl. Acad. Sci.*, **98,** 10533.

[10] Dyke, T. R., and Muenter, J. S., 1974, *J. chem. Phys.*, **60,** 2929.

[11] Dyke, T. R., 1977, *J. chem. Phys.*, **66,** 492.

[12] Dyke, T. R., Mack, K. M., and Muenter, J. S., 1977, *J. chem. Phys.*, **66,** 498.

[13] Odutola, J. A., and Dyke, T. R., 1980, *J. chem. Phys.*, **72,** 5062.

[14] Hougen, J. T., 1985, *J. molec. Spectrosc.*, **114,** 395.

[15] Odutola, J. A., Hu, T. A., Prinslow, D., O'dell, S, E., and Dyke, T. R., 1988, *J. chem. Phys.*, **88,** 5352.

[16] Coudert, L. H., and Hougen, J. T., 1988, *J. molec. Spectrosc.*, **130,** 86.

[17] Zwart, E., Termeulen, J. J., and Meerts, W. L., 1990, *Chem. Phys. Lett.*, **173,** 115.

[18] Zwart, E., Termeulen, J. J., Meerts, W. L., and Coudert, L. H., 1991, *J. molec. Spectrosc.*, **147,** 27.

[19] Fraser, G. T., 1991, *Int. Rev. phys. Chem.*, **10,** 189.

[20] Karyakin, E. N., Fraser, G. T., and Suenram, R. D., 1993, *Molec. Phys.*, **78,** 1179.

[21] Leforestier, C., Braly, L. B., Liu, K., Elrod, M. J., and Saykally, R. J., 1997, *J. chem. Phys.*, **106,** 8527.

[22] Fraser, G. T., Lovas, F. J., Suenram, R. D., Karyakin, E. N., Grushow, A., Burns, W. A., and Leopold, K. R., 1997, *J. molec. Spectrosc.*, **181,** 229.

[23] Paul, J. B., Provencal, R. A., and Saykally, R. J., 1998, *J. phys. Chem. A*, **102,** 3279.

[24] Braly, L. B., Liu, K., Brown, M. G., Keutsch, F. N., Fellers, R. S., and Saykally, R. J., 2000, *J. chem. Phys.*, **112,** 10314.

[25] Braly, L. B., Cruzan, J. D., Liu, K., Fellers, R. S., and Saykally, R. J., 2000, *J. chem. Phys.*, **112,** 10293.

[26] Goldman, N., Fellers, R. S., Brown, M. G., Braly, L. B., Keoshian, C. J., Leforestier, C., and Saykally, R. J., 2002, *J. chem. Phys.*, **116,** 10148.

[27] Keutsch, F. N., Braly, L. B., Brown, M. G., Harker, H. A., Petersen, P. B., Leforestier, C., and Saykally, R. J., 2003, *J. chem. Phys.*, **119**, 8927.

[28] Ojamae, L., and Hermansson, K., 1994, *J. phys. Chem.*, **98,** 4271.

[29] Hodges, M. P., Stone, A. J., and Xantheas, S. S., 1997, *J. phys. Chem. A*, **101,** 9163.

[30] Goldman, N., Leforestier, C., and Saykally, R. J., 2003, *J. chem. Phys.*, in preparation.

[31] Goldman, N., and Saykally, R. J., 2003, *J. chem. Phys.*, in preparation.

[32] Goldman, N., Fellers, R. S., Leforestier, C., and Saykally, R. J., 2001, *J. phys. Chem. A*, **105,** 515.

[33] Pfeilsticker, K., Lotter, A., Peters, C., and Bosch, H., 2003, *Science*, **300,** 2078.

[34] Vaida, V., Kjaergaard, H. G., and Feierabend, K. J., 2003, *Int. Rev. phys. Chem.*, **22,** 203.

[35] Vaida, V., and Headrick, J. E., 2000, *J. phys. Chem.* A, **104,** 5401.

[36] Aloisio, S., Francisco, J. S., and Friedl, R. R., 2000, *J. phys. Chem. A*, **104,** 6597.

[37] Goldman, N., 2003, personal communication.

[38] Keutsch, F. N., Goldman, N., Karyakin, E. N., Harker, H. A., Sanz, M. E., Leforestier, C., and Saykally, R. J., 2001, *Faraday Discuss.*, **118,** 79.

[39] Braly, L. B., 1999, PhD thesis, University of California at Berkeley, USA.

[40] Keutsch, F. N., Karyakin, E. N., Saykally, R. J., and van der Avoird, A., 2001, *J. chem. Phys.*, **114,** 3988.

[41] Liu, K., Fellers, R. S., Viant, M. R., McLaughlin, R. P., Brown, M. G., and Saykally, R. J., 1996, *Rev. sci. Instr.*, **67,** 410.

[42] Suenram, R. D., Fraser, G. T., and Lovas, F. J., 1989, *J. molec. Spectrosc.*, **138,** 440.

[43] Groenenboom, G. C., Wormer, P. E., S., van der Avoird, A., Mas, E. N., Bukowski, R., and Szalewicz, K., 2000, *J. chem. Phys.*, **113,** 6702.

[44] Smit, M. J., Groenenboom, G. C., Wormer, P. E. S., van der Avoird, A., Bukowski, R, and Szalewicz, K., 2001, *J. phys. Chem.* A, **105,** 6212.

[45] Mas, E. M., Bukowski, R., Szalewicz, K., Groenenboom, G. C., Wormer, P. E. S., and van der Avoird, A., 2000, *J. chem. Phys.*, **113,** 6687.
[46] Leforestier, C., 2003, personal communication.
[47] Fellers, R. S., Braly, L. B., Saykally, R. J., and Leforestier, C., 1999, *J. chem. Phys.*, **110,** 6306.
[48] Matsuoka, O., Clementi, E., and Yoshimine, M., 1976, *J. chem. Phys.*, **64,** 1351.